Probing metallization transitions in two-dimensional alkali metal films by metastable He-atom scattering

2004 J. Phys.: Condens. Matter 16 S2937

(http://iopscience.iop.org/0953-8984/16/29/009)

INSTITUTE OF PHYSICS PUBLISHING JOURNAL OF PHYSICS: CONDENSED MATTER

J. Phys.: Condens. Matter **16** (2004) S2937–S2952 PII: S0953-8984(04)80464-8

Probing metallization transitions in two-dimensional alkali metal films by metastable He-atom scattering

Gregor Witte

Physikalische Chemie I, Ruhr-Universität Bochum, 44780 Bochum, Germany

E-mail: witte@pc.rub.de

Received 4 May 2004
Published 9 July 2004
Online at stacks.iop.org/JPhysCM/16/S2937
doi:10.1088/0953-8984/16/29/009

Abstract

The survival probability of metastable He* atoms scattered from low work function materials depends sensitively on the electronic surface density of states which was utilized to characterize the degree of metallicity of ultrathin alkali metal (AM) films. By combining metastable He-atom scattering (MHAS) with He-atom scattering (HAS) to monitor the film growth, the coverage dependence of the metallization was studied. In this paper the metallization transition obtained for various AM (Na, K, Rb, Cs) and Ba films grown on Cu(100) and GaAs(100) surfaces are compared. It is shown that the onset of metallization observed for K, Cs and Ba on Cu(100) is in close agreement with a critical coverage estimated from a simple 2D Herzfeld model. Moreover, MHAS was also used to investigate the de-metallization of ultrathin AM films upon adsorption of O_2 or CO.

(Some figures in this article are in colour only in the electronic version)

1. Introduction

Thin-film materials that are normally considered as metals can exhibit behaviour that is very non-metallic. This phenomenon, which can occur even for films deposited on metal surfaces, has been observed in particular for dilute phases at submonolayer coverage where a non-metal to metal transition was found upon increasing coverage [1]. Theoretically, this behaviour has been studied extensively and various models have been proposed including Wilson, Peierls or Mott–Hubbard transitions [1]. On the other hand, the experimental determination of the metallicity of thin films is a rather difficult task due to the lack of a unique criterion of metallicity and because the supporting substrate usually hampers simple measurements of intrinsic film properties, for example their conductivity. Therefore in many studies the metallic character is probed indirectly by measuring related properties such as the appearance of film plasmon states or the density of states at the Fermi level.

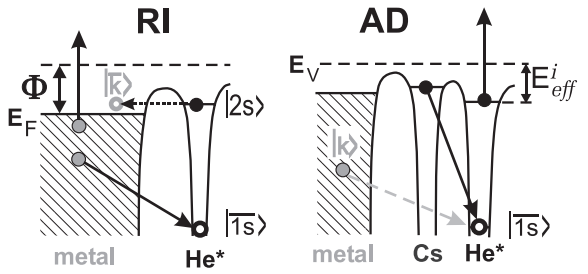

Figure 1. Schematic potential diagrams for the resonance ionization (RI) and Auger de-excitation (AD) in the presence of an alkali metal film.

A particularly interesting system in this respect represents the adsorption of alkali metal (AM) atoms on surfaces, which has been studied quite extensively since the pioneering experiments by Langmuir [2–6]. Because of their different electron affinity compared to (transition) metal substrates a significant fraction of the AM valence s electron is displaced towards the metal surface and thus creates a substantial dipole moment. With increasing coverage a mutual depolarization of these dipoles takes place and the AM atoms begin to form a metallic film. Since then this rather classical picture, originally proposed by Gurney [7], has been refined by realistic quantum theoretical calculations [6, 8, 9]. While the metallic character of a complete AM monolayer is well established [4] the metallization transition itself is difficult to observe experimentally. The direct observation of AM s valence state occupation by using ultraviolet photoelectron spectroscopy (UPS), the standard tool to study the electronic structure of adsorbate systems, is frequently hampered by the low density of states of the s band compared to the superimposed high density of states of the substrate at the Fermi level and additionally by the small photoemission cross section of s states [10].

These obstructions can partly be avoided by using metastable atom de-excitation spectroscopy (MDS), a unique surface sensitive electron spectroscopy pioneered by Ertl and coworkers [11–13] which meanwhile has been developed into a useful technique for probing surface electronic properties of adsorbate systems or liquid surfaces [14, 15]. While for the de-excitation of metastable He atoms (He*) on surfaces various mechanism have been identified [14], only some of them are of particular relevance for the experiments presented here.

On clean metal surfaces de-excitation of He* is dominated by the *resonance ionization* (RI) mechanism which is shown schematically in figure 1. In the first step the $He^*|2s\rangle$ electron is resonantly transferred to an empty surface state $|\overline{k}\rangle$, leaving a He^+ ion behind, which is neutralized in the second step by an Auger type transfer involving a filling of the $|\overline{1s}\rangle$ state and emission of a surface electron. If the work function, Φ, of the surface becomes smaller than the effective ionization energy of the metastable atom $E^i_{\rm eff}$ the RI process is suppressed because no unoccupied resonant states are accessible, and de-excitation only takes place via *Auger de-excitation* (AD). As depicted in figure 1 (right panel) the empty $He^*|\overline{1s}\rangle$ state is filled by a substrate surface electron and the $He^*|2s\rangle$ electron is emitted simultaneously in an Auger process, carrying the excess energy of the system. The most important feature of this process regarding the present experiment is its dependence on the electron density of states at the surface. In a first order approximation the de-excitation rate for this process $\Gamma_{\rm AD}$ is proportional to the overlap of the wavefunctions of the empty He $|\overline{1s}\rangle$ state and the filled state $|k\rangle$ of the surface [16]

$$\Gamma_{\rm AD} \propto \left|\langle\overline{1s}|k\rangle\right|^2. \tag{1}$$

Because the overall probability of He^* atoms surviving surface scattering in their metastable state is extremely small (typically 10^{-4}–10^{-6}), systematic He^* scattering experiments are challenging and were carried out only recently when intense He^* beams became available [17]. In a previous study we have demonstrated that a detailed analysis of the metallization transition of AM layers is also possible by using metastable He atom scattering (MHAS) [18]. In that approach the surviving He^* atoms are detected to investigate the changes in the electronic structure of the surfaces, while the diffracted ground-state He atoms provide additional information about the structure of the layer and their growth. A particular interesting model system for the study of metallization transitions are ultrathin AM films grown on Cu(100). Because the corrugation of that substrate is extremely small the submonolayer structures are mainly governed by the mutual repulsion between individual AM atoms which avoids agglomeration and thus provides a layer of continuously increasing density upon deposition [4, 5]. In this paper the metallization transitions obtained for various AM (Na, K, Rb, Cs) and Ba films grown on Cu(100) and GaAs(100) surfaces by using MHAS are compared. Moreover, this technique was applied to investigate the de-metallization of ultrathin AM films upon adsorption of O_2 or CO.

2. Experimental details

All experimental data which are summarized in this paper have been obtained by using two different UHV instruments: the lateral structure of the ultrathin films was characterized with a spot profile analysing (SPA) low energy electron diffraction (LEED) apparatus [19] and the He and He^* scattering experiments were performed with a HAS apparatus described in details elsewhere [17]. Essentially, an intense supersonic 2 $^3S_1$ He^* beam is produced by a cold discharge burning within the expansion zone. The discharge nozzle consists of a sapphire tube which on one side has a drilled nozzle orifice of 42 μm diameter. The discharge is driven by a high voltage applied between a thin tungsten tip cathode inside the tube and a nickel skimmer in front of the nozzle, resulting in a hot He^* beam with a typical kinetic energy of about 170 meV. By using a water-cooled tube jacket the beam energy which is almost equal for excited and non-excited He atoms (He and He^*) can be reduced to about $E_i \approx 100$ meV and a relative energy width of $\Delta E/E = 16\%$ is achieved. Under optimum conditions (3 mA discharge current and 1.5 bar nozzle pressure) the He^* flux typically amounts to 5×10^{15} $s^{-1}sr^{-1}$ and thus yields a relative population of metastable He atoms in the beam of 10^{-5}. When passing the He^* beam through an additional UV lamp to quench the 2 $^1S_0$ He^* singulet state, no change in the He^* beam intensity has been observed. This indicates the presence of an almost pure 2 $^3S_1$ He^* beam which is presumably caused by self-quenching due to UV-light emitted upon discharge [17]. As shown schematically in figure 2 the scattered He and He^* atoms can be detected independently by a magnetic mass spectrometer and a channeltron, respectively, mounted at fixed angles of 90° and 60° relative to the incident beam. By rotating the sample, angular distributions of the scattered atoms can be recorded. It should be emphasized that the UV-light produced upon discharge is also reflected at the sample surface and thus generates a substantial signal when entering the channeltron (especially close to specular conditions, see [17]). However, this obstruction is successfully suppressed by means of a velocity selector which has been added into the incident beam. Despite the large energetic width of the incident He beam upon burning discharge (which significantly exceeds the relative energy spread of high resolution supersonic He-beams of about 2%), sharp diffraction patterns can be obtained in the He angular distributions. This is illustrated for instance by an angular distribution recorded for a CO c(2 × 2) superstructure on Cu(100) shown in the inset in figure 2. In contrast to HAS the scattered He^* atoms reveal, however, only very broad angular distributions without any

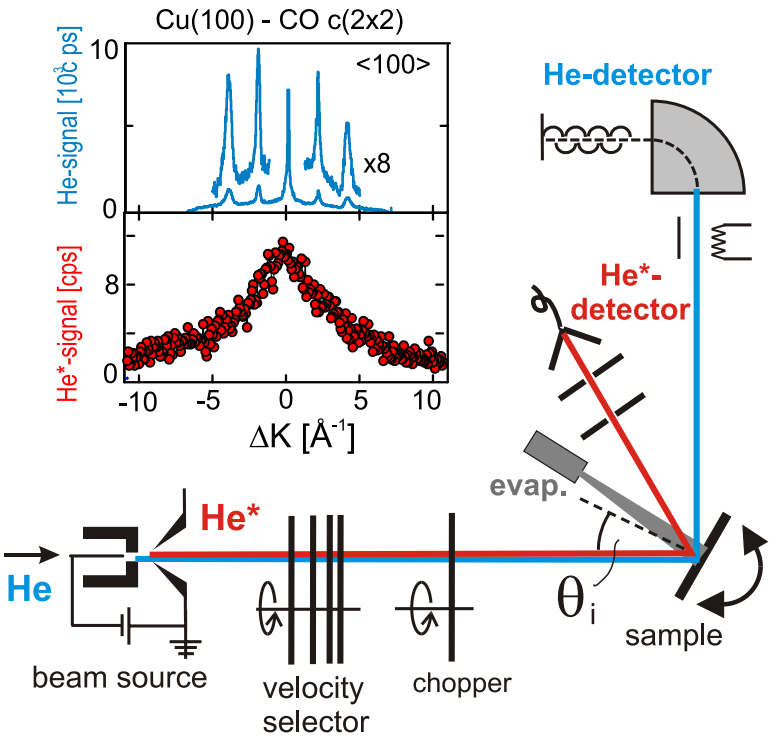

Figure 2. Schematic set-up of the MHAS apparatus with a metastable atom discharge source. The inset shows a comparison of typical He and He* angular distributions recorded along the ⟨100⟩ azimuth for a CO c(2 × 2) superstructure on Cu(100) with a discharge source ($k_i = 14$ Å^{-1}).

diffraction features. The same characteristic has also been observed for a number of different surfaces including various insulators (LiF, MgO and NiO), metals (Cu, Pd) or molecular adlayers (CO, NO/Pd and CO, alkanes/Cu) [20, 21]. The total He* survival probability was determined by integration of the He* angular distribution which yielded typical values between 8×10^{-6} and 8×10^{-7} [20]. These values were found to be approximately proportional to the He* signal at specular position. Therefore the intensity of the (still excited) scattered He* atoms can be recorded while measuring simultaneously the He atom specular reflectivity during exposure of the crystal (HAS growth curve) and thus allows us to measure the coverage dependence of the He* survival probability (MHAS growth curve).

In both instruments the Cu(100) and GaAs(100) samples were prepared *in situ* by standard cleaning procedures involving sputtering and annealing. These cycles were repeated until no traces of contamination were found in the Auger electron spectra and sharp diffraction peaks with a low diffuse background signal were observed in the LEED data or HAS angular distributions. Thin films of alkali metals (Na, K, Rb, Cs) or barium were prepared by evaporation from carefully out-gassed SAES getters dispensers at typical growth rates of 3–5 min/ML. To keep the pressure below 10^{-10} mbar during operation the dispenser were surrounded by a liquid nitrogen cooled copper shield. Moreover, prior to each film preparation the dispensers were preheated for about 15 min before opening the shutter to provide a constant flux during deposition. The oxygen and carbon monoxide gas (purity 99.997%) were dosed by backfilling the chamber through a leak valve to a pressure of about 5×10^{-8} mbar.

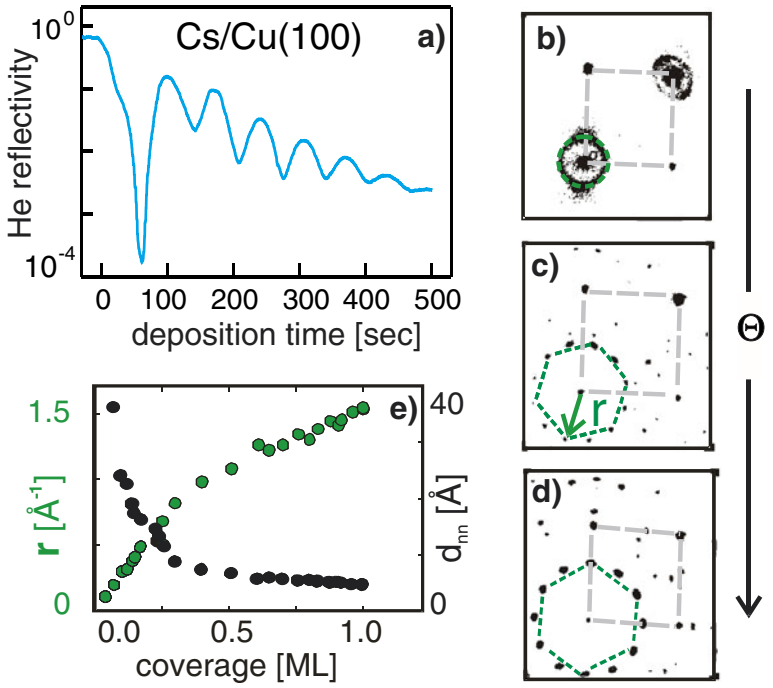

Figure 3. HAS growth curve for multilayer deposition of Cs/Cu(100) at 120 K (a), and (b)–(d) SPA-LEED diffraction pattern for various submonolayer phases with increasing coverage. The coverage dependence of the radius r obtained in the diffraction pattern is shown together with the nearest neighbour distance d_{nn} in panel (e).

3. Results

3.1. Alkali metal films on Cu(100)

The growth of alkali metal films (Na, K, Cs) was monitored by measuring the He atom reflectivity during deposition at a constant flux. As shown in figure 3(a) for the deposition of Cs on Cu(100) at a low substrate temperature of 120 K, the growth curves reveal characteristic intensity oscillations reflecting the completion of individual layers. The equidistant separation of the maxima indicates a layer-by-layer growth mode which has also been observed before for alkali metal films on various metal substrates (see e.g. [22]). Because of the large sticking probability of the evaporated AM atoms at low surface temperatures ($s \approx 1$) the actual submonolayer coverage can be determined through the deposition time relative to that for a full monolayer as indicated by the appearance of the first sharp oscillation maximum of the growth curve. The corresponding lateral structures of submonolayer films were characterized by additional LEED measurements. As an example, typical LEED patterns of submonolayer structures obtained for Cs/Cu(100) are shown in figure 3(b)–(d) [23]. Initially, at low coverage, ring-like diffraction patterns appear (figure 3(b)) for the different alkali metals which arise from *quasi-hexagonal* superstructures with appreciable azimuthal disorder but with a well defined nearest-neighbour spacing, d [24], while discrete hexagonal structures are formed at coverages above 0.5 ML. The corresponding unit cell size decreases with coverage (figures 3(c) and (d)) until finally a nearly hexagonal monolayer is formed. The average adatom separation d_{nn} in a hexagonal structure or the quasi-hexagonal phase is related to the radius r of the ring in

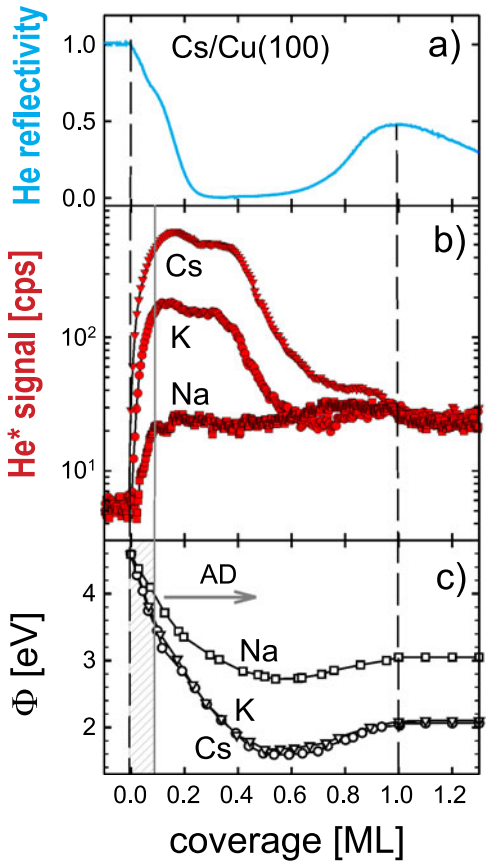

Figure 4. (a) HAS growth curve for the first Cs monolayer on Cu(100) and (b) He* signal recorded during monolayer deposition of various alkali metal atoms on Cu(100) at $T = 120$ K. The coverage dependent change of the work function [26] depicted in panel (c) shows that for coverages exceeding 0.1 ML de-excitation becomes possible only via Auger de-excitation (AD).

the diffraction pattern by $d_{nn} = 4\pi/\sqrt{3}r$. Coverage dependent measurements reveal further, that this adatom separation scales according to $d_{nn} = d_{\mathrm{ML}}\sqrt{\theta_{\mathrm{ML}}/\theta}$ (see figure 3(e)). The only exception is sodium which adopts various commensurate intermediate structures on Cu(100) before finally a c(2 × 2) monolayer phase is formed [25]. The resulting structures obtained for the various alkali metals are in good agreement with previous studies (for a detailed review on AM film structures see e.g. [5]). The corresponding monolayer coverages relative to the Cu(100) substrate, θ_{ML}, depend on the size of the AM atoms, and values of 0.50, 0.37 and 0.27 for Na, K and Cs, respectively have been derived from the diffraction data (see e.g. [5, 25, 26]).

Figure 4 compares the evolution of the He atom reflectivity and the intensity of the scattered He* atoms as a function of the AM coverage on the clean Cu(100) surface. Initially, a steep increase in the He* signal is obtained for all AMs which reaches a maximum at around 0.15 ML. The value of the maximal He* intensity depends on the size of the AM atoms and is largest in the case of Cs, where it is more than two orders of magnitude larger than for the clean Cu(100) surface. For K and Cs coverages of more than, 0.35 ML ($\theta_{\mathrm{K}} = 0.13$) and 0.40 ML ($\theta_{\mathrm{Cs}} = 0.11$) respectively, the He* signal starts to decrease strongly and reaches the same asymptotic value for a complete monolayer for all AMs which remains constant upon multilayer growth. Only for sodium does the He* signal reach the final level after the initial increase.

In a previous study the possible He* de-excitation channels have been discussed in detail [18] and the He* signal decay, which starts at about 0.4 ML, was ascribed to an onset of metallization of the AM films. Moreover, a model has been proposed in that study which

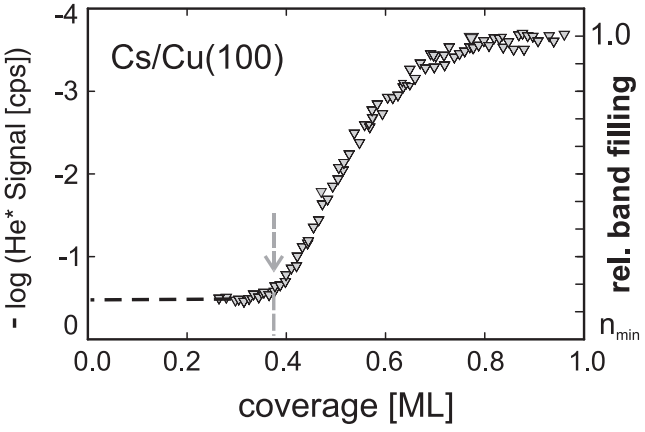

Figure 5. Relative occupation of the AM surface electronic states upon growth of a Cs monolayer obtained from the decrease of the scattered He^* signal by applying equation (2).

allows for a more *quantitative* interpretation of the MHAS data. At AM covered surfaces He^* atoms are predominantly de-excited via Auger de-excitation [14], i.e. by filling of the empty $He^*|\overline{1s}\rangle$-state with a surface electron. Therefore the surface density of states n projected onto the $|\overline{1s}\rangle$-state at a given coverage θ is, to a very good approximation, proportional to the de-excitation rate [16, 27], can be related to the reflected He^* intensity I_{He^*} by an exponential decay law [18]:

$$n(\theta) \propto -\log I_{He^*}(\theta). \tag{2}$$

Because this equation comes into effect only for an AD-process, it is limited to surfaces with a work function of less than about 3.5 eV, where a RI-process can be excluded [14]. Figure 5 displays the relative band filling, $n(\theta)$, for the case of Cs which starts to increase at about 0.4 ML (corresponding to a coverage of $\theta_{Cs} = 0.11$ relative to the substrate) and becomes saturated at 0.7 ML. For potassium a very similar curve was observed and reveals an onset of band filling at 0.35 ML ($\theta_K = 0.13$). From the corresponding diffraction patterns average nearest neighbour distances of $d_{nn}(K) = 8.5$ Å and $d_{nn}(Cs) = 7.6$ Å have been determined for the onset of metallization. Interestingly, the formation of azimuthally regularly ordered hexagonal overlayers of K and Cs takes place at slightly higher coverage of around $\theta = 0.17$. In contrast to that, the formation of ordered overlayers of sodium on Cu(100) already starts at a coverage of $\theta = 0.12$ [25]. The different behaviour observed for sodium can be related to a significantly shorter bond length with respect to the copper surface plane compared to the larger AM metals. This causes a very effective screening of the initial dipole moment and results in a smaller work function change compared to K or Cs, which is also reflected by the AM adatom vibrations [26]. Similar differences in the AM-substrate interaction were also reported in a previous *ab initio* study for K and Na on Al(111) [28].

3.2. Ba films on Cu(100)

Similar to the case of alkali metals a large reduction in the work function occurs also during deposition of alkaline earth metals (AEM) which in the case of barium can be as large as 3 eV. In contrast to AM the AEM films reveal, however, a larger thermal stability and have been employed in various applications such as cathodes for photoemission, thermionic energy converters or negative hydrogen ion sources in nuclear fusion technology [29, 30]. Considering the similarity of AM and AEM an interesting question arises in how far the growth and possible metallization transition of ultrathin AEM films parallels the scenario observed for AM films

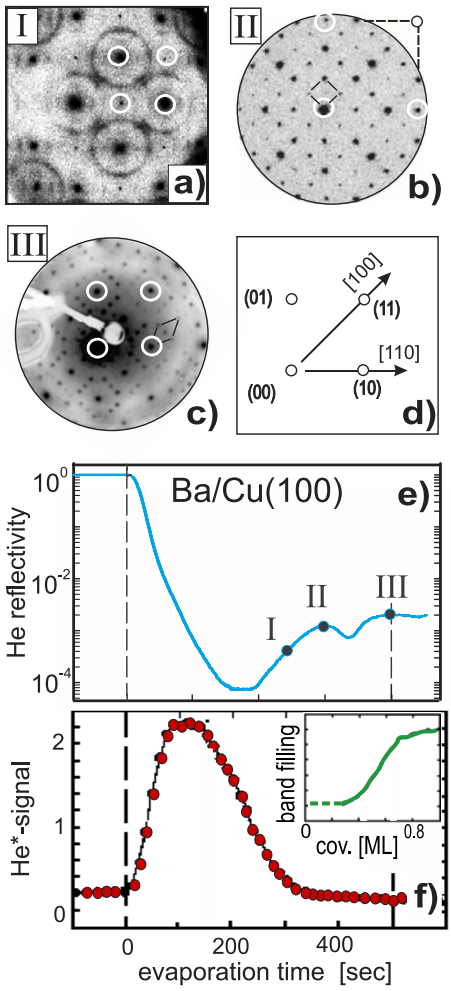

Figure 6. Summary of structural data measured upon formation of a Ba monolayer on Cu(100) at 450 K. The LEED patterns (a)–(c) obtained for various exposures, labelled I–III, are attributed to (a) a uniformly spaced phase, (b) a c(6 × 6) and (c) the c($4\sqrt{2} \times 2\sqrt{22}$)R45° monolayer structure. The corresponding HAS and MHAS growth curves are shown in panels (e) and (f) together with the resulting relative band filling derived from the decrease of the scattered He* signal (inset).

(described in the preceding section). To allow a direct comparison with the previous AM studies the growth of barium on Cu(100) was chosen as a model system. Despite the technological relevance the microscopic structure of AEM films are by far less extensively studied than that of the corresponding AM films. Therefore the geometrical structure and the growth of thin Ba films on Cu(100) has been characterized in a first step by using HAS and LEED [31]. It was found that below 200 K Ba films grow without any epitaxial ordering and only exhibit a weak quasi-hexagonal texture. With increasing temperature a thermally activated ordering was observed and for substrate temperatures above 350 K several ordered submonolayer phases were identified upon growth of the first monolayer; these are summarized in figure 6. Initially, at low coverage again a ring-like structure appears (phase I) which indicates a uniformly spaced structure. With increasing coverage azimuthally ordered structures are formed revealing an intermediate c(6 × 6) structure (phase II) and finally a c($4\sqrt{2} \times 2\sqrt{2}$)R45° monolayer structure (phase III).

From the corresponding ratio of the Auger signals for Ba and Cu a relative coverage of 0.26 was determined. A comparison with a coverage of $\theta = 0.125$ expected for a primitive c($4\sqrt{2} \times 2\sqrt{2}$)R45° structure suggests the presence of two Ba atoms per unit cell and thus

yields a monolayer coverage of $\theta = 0.25$. The relative deposition times for the appearance of the different phases (marked by I–III) are indicated in the corresponding HAS growth curve in figure 6(e). For the subsequent growth of a second Ba monolayer an incommensurate hexagonal structure has been identified which indicates a transition from a rather substrate mediated commensurate monolayer structure to a close packed Ba surface.

Figure 6 shows also a comparison of the corresponding HAS and MHAS growth curves for the first monolayer [32]. Similar to the growth of Cs on Cu(100) the He^* signal reveals initially a steep increase and decreases again above 0.4 ML. Unfortunately, the corresponding change of the work function could not be measured but related data have been reported for growth of Ba on Cu(111) [33]. This data show a rapid decrease of the work function of the clean copper surface with a maximal shift of -3 eV at about 0.3 ML followed by a weak increase reaching a work function shift of about -2.3 eV upon completion of the monolayer. A similar large decrease of the work function is also expected to occur on Cu(100) which implies identical He^* de-excitation channels as for the case of Cs. In turn this allows the application of equation (2) to approximate the relative band filling which yields virtually the same curve as for the case of Cs/Cu(100) (see inset in figure 6(f)). Additional experiments carried out for Ba deposition at various substrate temperatures between 130 and 500 K revealed no significant variation of the band filling curve [32].

3.3. Herzfeld criterion

The theoretical description of metallization transitions in solid states dates back to the beginning of the last century. A very simple model has been suggested by Goldhammer and Herzfeld to describe the density dependency of metal–insulator transitions [34]. In that model the valence electrons are considered as polarizable particles localized around the atomic ions thus providing an atomic polarizability α_0. With decreasing separation r the polarizability, however, starts to increase according to $[1 - (4\pi/3)(N_A/V_m)\alpha_0]^{-1}$, where V_m denotes the molar volume and N_A is Avogadro's constant. With increasing compression of the crystal lattice the polarizability finally diverges (*dielectric catastrophe*) which can be interpreted as a delocalization of the valence electrons and hence metallicity. The so-called Herzfeld criterion relates the appearance of metallization to a critical density N_A/V_m by

$$\frac{4\pi}{3}\frac{N_A}{V_m}\alpha = 1. \tag{3}$$

Although this criterion is derived from classical considerations, it can be related to quantum mechanics by realizing that for hydrogen-like atoms (such as AM or AEM) the atomic polarizability scales approximately with the radius of the s-orbitals r_s according to $\alpha \approx r_s^3$. Thus the valence orbitals start to overlap when equation (3) is fulfilled.

A corresponding criterion can also be formulated for two dimensions, e.g. for thin films. In that case the critical density has to be replaced by a critical coverage, θ_M, where metallization occurs. For a quadratic surface lattice with a lattice constant a the effective surface per adatom at this critical coverage is given by a^2/θ_M and thus yields a corresponding Herzfeld criterion for 2D:

$$\frac{\pi\theta_M}{a^2}\alpha^{2/3} = 1. \tag{4}$$

Experimental data for the critical coverages of metallization have been derived from MHAS data by using coverages at which the relative band filling amounts to 50% of the monolayer value (K: 0.45 ML, Cs: 0.60 ML and Ba: 0.55 ML) and considering the corresponding relative monolayer coverages θ_{ML}. The resulting values are summarized in

Table 1. Comparison of critical coverages θ_M for the metallization transition of K, Cs and Ba films on Cu(100) obtained from MHAS experiments and according to equation (4).

	K	Cs	Ba
Lattice constant (Å)	5.33	6.05	5.01
α (Å^3)	37	50	41
θ_M Herzfeld	0.19	0.15	0.17
θ_M experiment	0.17	0.16	0.14
θ_{ML} at Cu(100)	0.37	0.27	0.25

table 1 and compared with the critical densities of metallization expected from the 2D Herzfeld criterion for the various AM and AEM films on Cu(100) ($a_{Cu} = 2.55$ Å). Although the model is rather simple, a surprisingly close agreement with the experimental data is observed. A comparison with the corresponding layer structures obtained by LEED shows further that, within the experimental resolution ($\Delta\theta \approx \pm 0.03$), the metallization coincides with the appearance of azimuthally ordered structures.

3.4. Alkali metal films on GaAs(100)-(4 × 2)

In contrast to metal substrates the adsorption of thin AM layers on semiconductor surfaces is mainly stabilized by localized interactions with the dangling bonds of the substrate [6] and has been studied quite extensively because it is considered as a model system for Schottky barriers [6, 35]. Experimental evidence for a Mott insulator state of Cs on the GaAs(110) cleavage surface was reported [36, 37], whereas with increasing coverage the formation of metallic bands was found which can be described by a Mott–Hubbard metallization transition [1]. In view of these transitions we have applied MHAS to characterize also the growth and metallization behaviour of AM films on GaAs(100) [38]. This surface was chosen because it can be prepared repeatedly by sputtering and annealing which yields the well known gallium terminated (4 × 2) reconstruction. Moreover, the adsorption of alkali metals on that surface had been studied before quite extensively (see e.g. [39] and references therein). Moreover, MDS experiments have been carried out for Cs/GaAs(100) [40] and hence allow a direct comparison with the MHAS experiments.

Previous experiments based on Auger electron spectroscopy have shown that the growth of Cs layers on GaAs(100) depends critically on the substrate temperature and coverage [39]. It was found that the sticking coefficient drops significantly when exceeding a coverage of 0.5 ML and decreases strongly with increasing temperature. As a consequence at room temperature no saturated Cs monolayer can be grown while it is stable at low temperatures only. Such growth properties have also been observed in the corresponding HAS data. Figure 7(a) summarizes different HAS growth curves obtained for various alkali metals (K, Rb and Cs) and for Cs deposition at different substrate temperatures. For low substrate temperatures (below 200 K) characteristic growth oscillations are seen which reveal a distinct maximum corresponding to the completion of the monolayer. While the He reflectivity reveals no further variation and thus no additional uptake at elevated temperatures (as shown for Cs). This in accordance with previous AES experiments [39] which show that a complete Cs monolayer can be formed only at temperatures below about 250 K. The corresponding structural analysis based on HAS angular distributions revealed that a (4 × 2) superstructure seen for the clean surface is also maintained at 0.5 ML, while upon subsequent exposure the diffraction pattern disappeared completely. This is in close agreement with previous results where it has been suggested that the adsorption on that reconstructed surface proceeds in two steps [39]: first the topmost

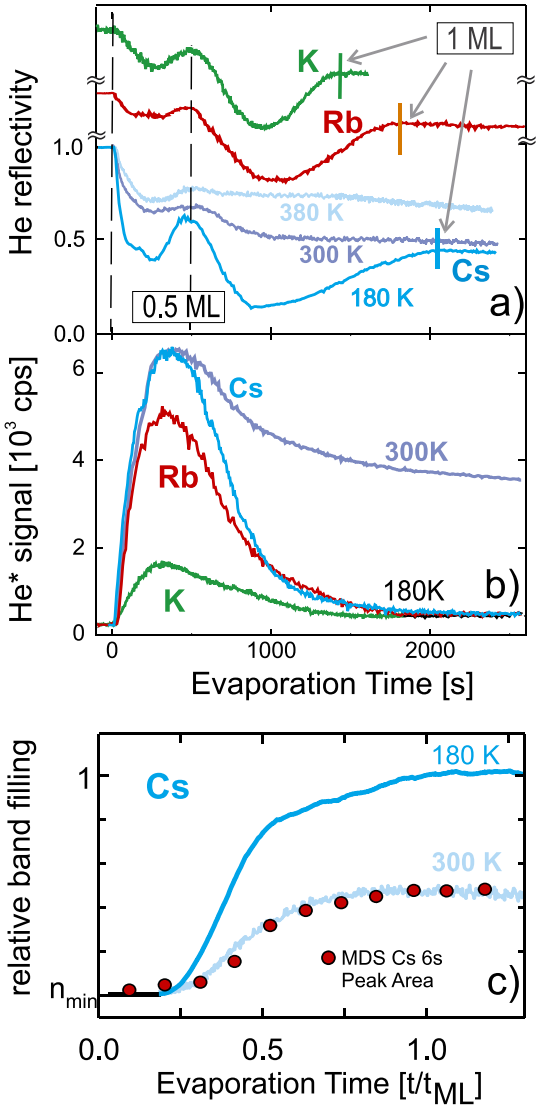

Figure 7. (a) HAS growth curves recorded during deposition of various AM on GaAs(100)-(4 × 2) at 180 K. For comparison additional growth curves of Cs are shown for different temperatures. The corresponding MHAS curves are displayed in panel (b) from which a relative band filling (c) has been derived. The latter curve is also compared directly with the Cs 6s peak intensities obtained from MDS data by Nishigaki *et al* [40] as a function of evaporation time.

Ga-dimers are occupied and subsequently also the troughs are filled which is accompanied by formation of a laterally disorder saturated monolayer.

As shown in figure 7(b) the corresponding MHAS curves again revealed a characteristic signature with an initial increase followed by a subsequent decay starting when exceeding a coverage of 0.5 ML and reach the same monolayer value for all studied alkali metals (K, Rb, Cs). As a consequence of the reduced sticking coefficient at elevated temperature no complete drop of the He^* intensity was observed as demonstrated by a Cs deposition at room temperature. Although the work function of the clean GaAs(100) surface is rather large and amounts to $\Phi = 5$ eV it decreases rapidly to below 3.5 eV at about 0.1 ML Cs and reaches a value of 2.1 eV at a complete monolayer [39]. When interpreting the MHAS data it has to be considered that a further de-excitation channel, involving a resonant charge transfer from the surface to the He^* atom (RI + autodetachment), becomes energetically possible near the minimum of the

work function [14]. However, its appearance has been excluded experimentally [40] based on MDS data for the case of Cs, which exhibits the lowest work function minimum among the investigated AMs and hence equation (2) can be applied to K and Rb as well. The results of this analysis are compared in figure 7(c) for Cs films deposited at different temperatures. Also shown is the intensity of the Cs 6s peak obtained from the room temperature MDS data by Nishigaki *et al* [40], the height of which has been adapted to the MHAS curve at the completion of the monolayer t_{ML}. The very close agreement of both curves thus confirms the applicability of the present evaluation procedure.

For all of the examined AMs, the metallization is only complete upon completion of the first monolayer. Moreover, systematic measurements have shown that for adsorption of Cs at surface temperatures of more than 250 K, the electron density at the saturation coverage ($\theta < 1$ ML as confirmed by HAS) was found to be much lower than for the low temperature layers (see figure 7(b)). This indicates that no metallization is reached at elevated temperatures. In a recent EELS study of Cs adsorption on GaAs(100) an increase of the Ga 3d peak was seen during Cs evaporation at 200 K, while at 300 K no such increase could be detected. This has been interpreted as proof that the Cs saturation coverage is metallic only at 200 K or below, in line with the present findings.

3.5. De-metallization through coadsorption

It has been shown in several studies that subsequent adsorption of oxygen or carbon monoxide on metallic AM layers deposited on Ru(0001) or Cu(110) causes a de-metallization which was attributed to a formation of covalent bonds at the cost of a depopulation of the AM valence band [10, 41–43]. By using HREELS the disappearance of the Cs–Ru vibration upon metallization and its reappearance due to the de-metallization was observed [41]. A more direct evidence of the successive emptying of the Cs 6s state was obtained in MDS studies. In the case of a Cs monolayer deposited on Cu(110) the complete disappearance of the Cs 6s signal was observed after an oxygen exposure of 0.5 L (1 Langmuir $= 10^{-6}$ Torr s) [10, 43]. A similar behaviour was also observed for Cs pre-covered Ru(0001) after exposing the surface to CO [42]. Motivated by these results the adsorption of O_2 and CO on thin AM films was also studied by MHAS [38, 44].

Figure 8 compares the variation of the He reflectivity and the simultaneously measured He^* signal for a potassium monolayer on Cu(100) upon exposure to oxygen or carbon monoxide at a surface temperature of 120 K. The initial adsorption of molecules is sensitively monitored by the measured HAS reflectivity and yields significant differences in the sticking coefficients for CO and O_2. While the potassium surface is saturated to oxygen already after a dosage of 1 L a saturated CO layer is formed only after an exposure of about 100 L. The corresponding He^* signals run opposite and reveal an increasing survival probability with increasing adsorbate coverage. To explain this data various mechanisms including geometrical screening, autodetachment or a reduction of the density of states of the AM valence band have been considered [38, 44] but the former two mechanism were ruled out (see below). Since the MHAS signal reflects the electronic density at the vacuum side of the surface, the He^* signal increase indicates a re-polarization of the outermost surface, which depletes the number of electrons accessible for de-excitation of He^*. Additional information has been derived by monitoring the adsorption of oxygen on different AM monolayers (Na, K, Cs). As displayed in figure 9(a) the asymptotic He^* signal that is reached at an exposure of about 10 L was found to increase with the size of the AM atoms. Only a slight decrease of the He^* signal was found during oxygen exposure of the clean copper surface which can be attributed to an increase of the RI rate. Interestingly, the asymptotic He^* signals of the AM films obtained

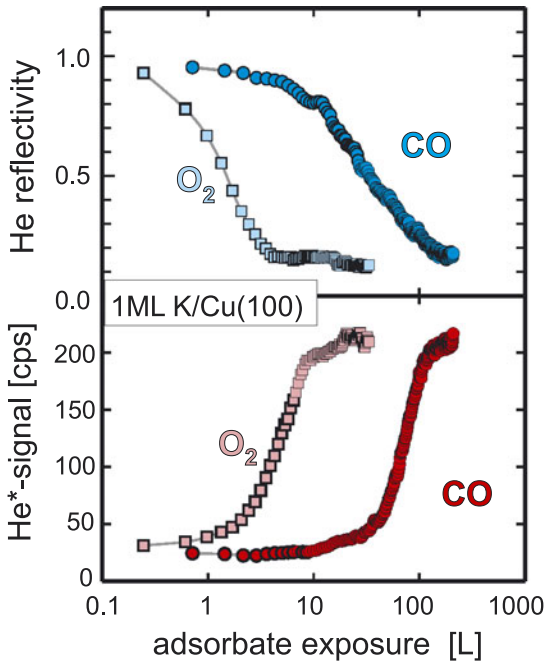

Figure 8. HAS reflectivity and scattered He^* signal recorded during exposure of a potassium monolayer/Cu(100) to oxygen and carbon monoxide at 120 K.

for large exposure are virtually identical to the maximal He^* signals which were observed for the non-metallic submonolayer AM films at about 0.15 ML (see figure 4(b)) and thus can be attributed to a partial de-metallization of the alkali metal monolayer upon oxygen adsorption. In the case of Cu(110) a de-metallization of a Cs monolayer was already seen after an oxygen exposure of about 0.5 L [10] as opposed to 10 L in the present case. This difference can be explained by the more open geometry of the Cs monolayer on Cu(110) [5] compared to the very smooth Cs film grown on Cu(100) [18], which facilitates the oxygen uptake.

Finally, we close this section with a brief description of MHAS experiments on coadsorption of oxygen and AM films grown on a semiconductor surface, namely GaAs(100) [38]. A particular interest in this system arises from the fact that the coadsorption of caesium and oxygen on GaAs surfaces causes a shift of the vacuum level below the conduction band (*negative electron affinity*, NEA). This is exploited in the production of efficient photocathodes and, in particular, in combination with GaAs(100) surfaces is used as emitters of spin-polarized electrons [35, 45]. Because of the absence of any crystalline order for both the clean AM films and the AM/O films on GaAs(100), no further structural information could be derived from HAS or LEED. Figure 9(b) summarizes a set of corresponding He^* curves recorded upon oxygen uptake on monolayer films of K, Rb and Cs grown on GaAs(100)-(4×2) at a temperature of 180 K. The situation parallels that obtained for AM on Cu(100) and the He^* signal reveals a sudden increase at an exposure of about 0.3 L and reaches a constant value above 10 L. In the case of Cs, however, the MHAS curve reveals an additional distinct minimum at an oxygen exposure of about 0.75 L before the same signal increase and levelling above 10 L appears as for K and Rb [38]. The increase of the He^* signal is again interpreted as a de-metallization, which in that case is in accordance with the results of a recent MDS study, where the depletion of the Cs 6s states upon oxygen exposure was observed directly [46]. As regards the minimum observed in the MHAS growth curve for the Cs layer there are generally two possible explanations for this effect. On the one hand, this

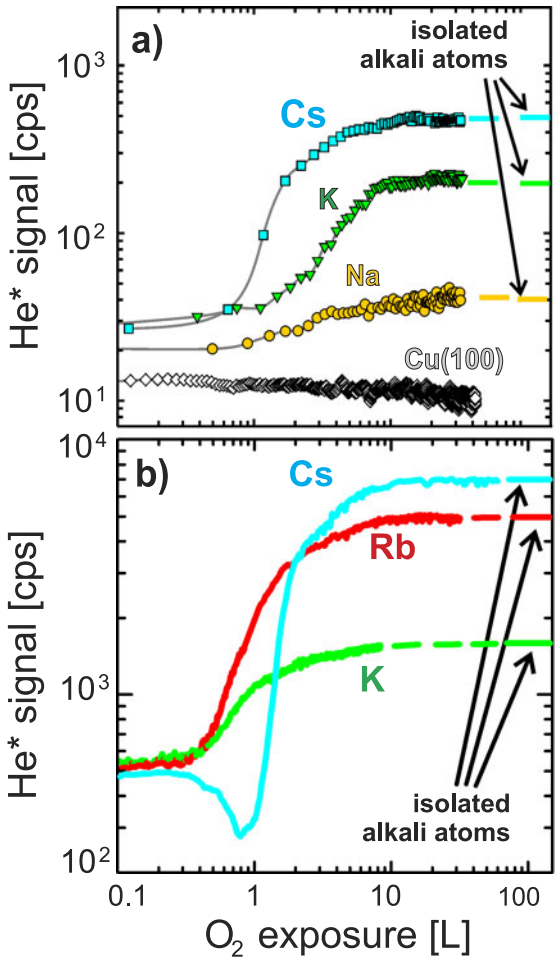

Figure 9. Evolution of the scattered He^* signal upon oxygen exposure of different AM monolayer films grown on (a) Cu(100) and (b) GaAs(100) surfaces.

behaviour may be understood in terms of a polarization at the surface with a sign opposite to the polarization that is due to initial AM adsorption, i.e. it is accompanied by an enhancement of the electron density at the vacuum side of the surface. On the other hand it is possible that such an additional de-excitation is caused by a resonant ionization/autodetachment process which can occur at low work functions. The MDS spectra for the coadsorption of oxygen and caesium indicate, however, that the latter channel is negligible [46]. Therefore, the appearance of the He^* intensity minimum is attributed to an increase of the electron density. Using ultraviolet photoemission spectroscopy Araghi-Kozaz *et al* [47] have shown that during oxygen adsorption on a Cs covered GaAs(100) surface, initially a peroxo (O_2^{2-}) species appears which transforms into a superoxo (O_2^-) species upon further exposure. This transition was found to occur at 1 L, which is about the minimum of the presently measured MHAS curve. Since the impinging He^*-atoms see only the electronic density of the outermost layer, our findings thus indicate that the peroxo species, which dominates up to about 1 L, is located at or on top of the AM layer, whereas the superoxo species, dominating at higher exposures, is situated at sites which are not exposed by the impinging He^*, i.e. subsurface. Araghi-Kozaz *et al* suggested further that the appearance of superoxo and the GaAs–O formation, i.e. the onset of substrate oxidation, are linked together, which is supported by the MHAS data. The strict surface sensitivity of

MHAS indicates further that this transition is also accompanied by a change of the structural arrangement of the surface atoms: at the work function minimum the oxygen submerges and starts substrate oxidation.

4. Conclusions

In summary the presented MHAS studies demonstrate that the high sensitivity of the metastable He^* de-excitation rate on the electronic surface structure can be used to characterize the formation of metallic thin films which have a sufficiently low work function to suppress a de-excitation by resonance ionization. By combining the extreme surface sensitivity of MHAS to detect modifications of the electronic surface structure with the high sensitivity of ground state HAS for measuring the coverage during AM film growth, details on the coverage dependence of the metallization transition occurring from an initially dilute phase of polarized isolated AM atoms towards a metallic monolayer were derived. It was further shown that also the reverse process, namely a de-metallization caused by subsequent oxygen adsorption, can be monitored by MHAS. At present, however, a detailed picture of the He^*–surface interaction, in particular for non-de-excited atoms, has not yet emerged and deserves further investigation. In particular a more quantitative analysis of the He^* intensities is presently limited by the lack of a theoretical framework. In a recent *ab initio* study Bonini *et al* [48] have calculated the de-excitation rates of He^* scattered from a Na surface and observed a close agreement with the experimental MHAS data. Hopefully, this will stimulate further theoretical work.

Acknowledgment

This work has been funded by the Deutsche Forschungsgemeinschaft DFG (contract Wi 1361-3/3)

References

[1] Dowben P A 2000 *Surf. Sci. Rep.* **40** 151
[2] Langmuir I and Kingdon K H 1923 *Phys. Rev.* **21** 380
[3] Langmuir I 1932 *J. Am. Chem. Soc.* **54** 2798
[4] Aruga T and Murata Y 1989 *Prog. Surf. Sci.* **31** 61
[5] Diehl R D and McGrath R 1996 *Surf. Sci. Rep.* **23** 43
[6] Bechstedt F and Scheffler M 1993 *Surf. Sci. Rep.* **18** 145
[7] Gurney R W 1935 *Phys. Rev.* **47** 479
[8] Ishida H 1990 *Phys. Rev.* B **42** 10899
[9] Bagus P S and Pacchioni G 1993 *Phys. Rev. Lett.* **71** 206
[10] Woratschek B, Sesselmann W, Küppers J, Ertl G and Haberland H 1987 *J. Chem. Phys.* **86** 2411
[11] Conrad H, Ertl G, Küpers J, Sesselmann W and Haberland H 1982 *Surf. Sci.* **121** 161
[12] Woratschek B, Sesselmann W, Küppers J, Ertl G and Haberland H 1987 *Surf. Sci.* **180** 187
[13] Sesselmann W, Woratschek B, Küppers J, Ertl G and Haberland H 1987 *Phys. Rev.* B **35** 1547
[14] Harada Y, Masuda S and Ozaki H 1997 *Chem. Rev.* **97** 1897
[15] Morgner H 2000 *Advances in Atomic Molecular and Optical Physics* vol 42 (San Diego, CA: Academic) pp 387–488
[16] Sesselmann W, Woratschek B, Ertl G, Küppers J and Haberland H 1984 *Surf. Sci.* **146** 17
[17] Fouquet P, Day P K and Witte G 1998 *Surf. Sci.* **400** 140
[18] Fouquet P and Witte G 1999 *Phys. Rev. Lett.* **83** 360
[19] Braun J, Toennies J P and Witte G 1995 *Surf. Sci.* **340** 265
[20] Fouquet P and Witte G 1999 *Surf. Rev. Lett.* **6** 103
[21] Fouquet P 1996 *Diploma Thesis* University Göttingen, Max-Planck-Institut für Strömungsforschung (Report 16/1996)

[22] Hulpke E, Lower J and Reichmuth A 1996 *Phys. Rev.* B **53** 13901
[23] Witte G 1995 *Dissertation* University Göttingen, Max-Planck-Institut für Strömungsforschung (Report 8/1995)
[24] Gerlach R L and Rhodin T N 1969 *Surf. Sci.* **17** 32
[25] Graham A P and Toennies J P 1997 *Phys. Rev.* B **56** 15378
[26] Senet P, Toennies J P and Witte G 1999 *Chem. Phys. Lett.* **299** 389
[27] Kantorovich L N, Shluger A L, Sushko P V and Stoneham A M 2000 *Surf. Sci.* **444** 31
[28] Neugebauer J and Scheffler M 1992 *Phys. Rev.* B **46** 16067
[29] Tuck R A 1983 *Vacuum* **33** 715
[30] Van Os C F A, van Amersfoot P W and Los J 1988 *J. Appl. Phys.* **64** 3863
[31] Bartholmei S, Fouquet P and Witte G 2001 *Surf. Sci.* **473** 227
[32] Bartholmei S 1999 *Diploma Thesis* University Göttingen
[33] Lindgren S A and Wallden L 1991 *Surf. Sci.* **257** L619
[34] Herzfeld K F 1927 *Phys. Rev.* **29** 701
[35] Batra I P 1989 *Metallization and Metal–Semiconductor Interfaces* (*NATO ASI Series B* vol 195) (New York: Plenum)
[36] DiNardo N J, Maeda-Wong T and Plummer E W 1990 *Phys. Rev. Lett.* **65** 2177
[37] Whitman L J, Stroscio J A, Dragoset R A and Celotta R J 1991 *Phys. Rev. Lett.* **66** 1338
[38] Fouquet P and Witte G 2001 *Appl. Surf. Sci.* **180** 286
[39] Kamaratos M and Bauer E 1991 *J. Appl. Phys.* **70** 7564
[40] Nishigaki S, Yamada K, Asanari J and Naitoh M 1998 *Ultramicroscopy* **73** 223
[41] Jacobi K, Shi H, Gruyters M and Ertl G 1994 *Phys. Rev.* B **49** 5733
[42] Fichtner-Endruschat S, De Renzi V, Morgante A, Schwegmann S, Bludau H, Schuster R, Böttcher A and Over H 1998 *J. Chem. Phys.* **108** 774
[43] Woratschek B, Ertl G, Küppers J, Sesselmann W and Haberland H 1986 *Phys. Rev. Lett.* **57** 1484
[44] Fouquet P and Witte G 2000 *Surf. Sci.* **454–456** 256
[45] Tang F C, Lubell M S, Rubin K, Vasilakis A, Eminyan M and Slevin J 1986 *Rev. Sci. Instrum.* **57** 3004
[46] Yamada K, Asanari J, Naitoh M and Nishigaki S 1998 *Surf. Sci.* **402–404** 683
[47] Araghi-Kozaz H, Brojerdi G, Besançon M, Dolle P and Jupille J 1991 *Surf. Sci.* **251/252** 1091
[48] Bonini N, Brivio G P and Trioni M I 2003 *Phys. Rev.* B **68** 035407